Molecular Biology of the Cell
Vol. 19, 2553–2565, June 2008

RAB-11 Permissively Regulates Spindle Alignment by Modulating Metaphase Microtubule Dynamics in *Caenorhabditis elegans* Early Embryos

Haining Zhang,*† Jayne M. Squirrell,† and John G. White†‡

*Laboratory of Genetics, †Laboratory of Molecular Biology and ‡Department of Anatomy, University of Wisconsin, Madison, WI 53706

Submitted September 6, 2007; Revised March 18, 2008; Accepted March 24, 2008
Monitoring Editor: Sean Munro

Alignment of the mitotic spindle along a preformed axis of polarity is crucial for generating cell diversity in many organisms, yet little is known about the role of the endomembrane system in this process. RAB-11 is a small GTPase enriched in recycling endosomes. When we depleted RAB-11 by RNAi in *Caenorhabditis elegans*, the spindle of the one-cell embryo failed to align along the axis of polarity in metaphase and underwent violent movements in anaphase. The distance between astral microtubules ends and the anterior cortex was significantly increased in *rab-11(RNAi)* embryos specifically during metaphase, possibly accounting for the observed spindle alignment defects. Additionally, we found that normal ER morphology requires functional RAB-11, particularly during metaphase. We hypothesize that RAB-11, in conjunction with the ER, acts to regulate cell cycle–specific changes in astral microtubule length to ensure proper spindle alignment in *Caenorhabditis elegans* early embryos.

INTRODUCTION

The first cell division of the *Caenorhabditis elegans* zygote (P0) is asymmetric, giving rise to two daughter cells with different sizes and fates: the smaller P1 cell inherits germline determinants such as PIE-1 (Mello *et al.,* 1996) and the larger AB cell develops into most of the somatic tissues (Sulston *et al.,* 1983). This asymmetric division requires two well-regulated spindle alignment phases. First, before metaphase, the centrosomal-nuclear complex migrates to the center of the embryo while undergoing a 90° rotation to align the mitotic spindle onto a preformed A-P axis defined by the axially segregated PAR proteins (Cowan and Hyman, 2004a). This rotational alignment depends on the interactions of astral microtubules (MTs) with cortical regulators such as dynein-dynactin (Skop and White, 1998; Gonczy *et al.,* 1999a) and the DEP domain protein LET-99 (Tsou *et al.,* 2002). In the second phase, the redundant G_{α}proteins, GOA-1 and GPA-16, transduce the polarity cues of the PAR proteins into forces that displace the spindle posteriorly during anaphase (Gotta and Ahringer, 2001; Tsou *et al.,* 2003). Although G_{α}distributes uniformly around the cortex (Gotta and Ahringer, 2001), its upstream activator, GPR-1/2, localizes asymmetrically in response to the PARs: it is enriched on the posterior cortex where PAR-2 is localized and reduced on the anterior cortex where PAR-3 is localized (Colombo *et al.,* 2003; Gotta *et al.,* 2003). The activity of Gα is down-regulated by G$\beta\gamma$ and LET-99, possibly by reducing the level of GPR-1/2 on the cortex (Tsou *et al.,* 2003). Although little is known about the downstream effectors of Gα, it has been hypothesized that the minus-end MT motor dynein-dynactin might be the force generator activated by Gα (Grill *et al.,* 2003). Both the rotation of the spindle and the posterior spindle displacement at anaphase are dependent on the cortical PAR polarity (Colombo *et al.,* 2003), together with region-specific cortical interactions with astral MTs. Mutations in genes that result in short astral MTs, such as *tbb-2* (tubulin β-subunit; Wright and Hunter, 2003), *zyg-8* (a doublecortin-related kinase; Gonczy *et al.,* 2001), and *zyg-9* (the XMAP215 ortholog; Matthews *et al.,* 1998), all fail to align the mitotic spindle properly. How MT length is regulated during the cell cycle in order to execute different spindle alignment processes is not well understood.

A factor that might contribute to the regulation of spindle alignment is membrane trafficking. Studies in *Fucus* (Shaw and Quatrano, 1996) and the EMS cell of *C. elegans* (Skop *et al.,* 2001) have shown that treating the embryos with the secretion inhibitor brefeldin A (BFA) inhibits rotational alignment of the spindle. In the case of *C. elegans*, it is not clear whether BFA prevents spindle rotation in the EMS cell by perturbing the P2/EMS signaling (such as Wnt and MES-1/SRC-1 pathways) that act to polarize EMS (Walston and Hardin, 2006) or by affecting the spindle alignment process directly. Furthermore, when either of two *C. elegans* ER proteins, OOC-3 (a putative transmembrane protein) and OOC-5 (a Torsin-related AAA ATPase), are mutated, the majority of the embryos exhibit P1 spindle rotation defect, caused by either disrupting the polarization of the P1 cell or the organization of actin cytoskeleton at the midbody remnant (Pichler *et al.,* 2000; Basham and Rose, 2001).

To understand further how membrane trafficking may affect spindle alignment, we examined the functions of the Rab family proteins in *C. elegans* one-cell embryos (P0) in which spindle alignment is cell autonomous (Goldstein,

This article was published online ahead of print in *MBC in Press* (http://www.molbiolcell.org/cgi/doi/10.1091/mbc.E07–09–0862) on April 2, 2008.

Address correspondence to: John G. White (jwhite1@wisc.edu).

Abbreviations used: A-P, anterior-posterior; RNAi, RNA interference; Gα, α subunit of the trimeric G protein; G$\beta\gamma$, β and γ subunit of the trimeric G protein; MT, microtubule; WT, wild-type; Δ, deletion.

2000) and is well studied (Cowan and Hyman, 2004a). Rab proteins regulate the specificity of membrane trafficking by localizing to the cytosolic surface of distinct membrane compartments and facilitating all stages of membrane trafficking, including vesicle budding, cargo sorting, transport, tethering, and fusion (Zerial and McBride, 2001). In this report, we focus on Rab11, which localizes to recycling endosomes (RE) and is required for both constitutive and regulated protein recycling from RE to the plasma membrane (PM), as well as transporting de novo synthesized proteins from the *trans*-Golgi network (TGN) to the PM in mammalian cells (Prekeris, 2003). Rab11 achieves its function by interacting with Rab11-FIPs (Rab11 family of interacting proteins; Prekeris, 2003), which colocalize to RE with Rab11 (Hales *et al.*, 2001; Lindsay *et al.*, 2002; Wallace *et al.*, 2002; Horgan *et al.*, 2004). In addition to regulating endocytic recycling, Rab11 is involved in several cellular functions, such as cell migration and cytokinesis (Skop *et al.*, 2001; Pelissier *et al.*, 2003; Jones *et al.*, 2006). Both events require coordination between targeted delivery and fusion of membranes as well as cytoskeletal rearrangements. Rab11 has been shown to function in membrane trafficking but whether it is involved directly or indirectly in the cytoskeletal rearrangements in these processes is not known. Recent studies have shown that Rab11 can indeed affect the cytoskeleton. In *Drosophila*, Rab11 organizes MT plus ends during oogenesis (Dollar *et al.*, 2002) and remodels the actin cytoskeleton during cellularization (Riggs *et al.*, 2003), although the detailed mechanisms are unknown. Our study identifies a new role for RAB-11 (the *C. elegans* ortholog of mammalian Rab11a) in regulating the cytoskeleton, namely to facilitate astral MT elongation during metaphase to ensure proper spindle alignment in the first cell division. Also, we show that RAB-11 is required for the normal endoplasmic reticulum (ER) morphology during metaphase.

MATERIALS AND METHODS

C. elegans Strains

All worm strains were maintained as described (Brenner, 1974). The following strains were used: N2: wild type (WT), WH0204: *unc-119(ed3); ojIs1[beta-tubulin::GFP unc-119(+)]*, WH0327: *unc-119(ed3); ojIs23[SP12::GFP unc-119(+)]*, WH0347: *unc-119(ed3); ojIs35 [rab-11.1:: GFP unc-119(+)]*, TH66: EBP-2::GFP, WH0258: *unc-119(ed3); ojIs5[dnc-2::GFP unc-119(+)]*, DH235: *zyg-8 (b235)III*, SP432: *unc-4(e120) ooc-3(mn241)/mnC1 dpy-10(e128) unc-52(e444)II* (Kemphues *et al.*, 1988), and KK696: *ooc-5(it145) unc-4(e120)/mnC1 dpy-10(e128) unc-52(e444) II*. We grew SP432 (*ooc-3(mn241)*) and KK696 (*ooc-5(it145)*) worms at 16°C and used the uncoordinated worms, which are homozygous for the mutations for analysis. DH235 (*zyg-8 (b235)*) was also maintained at 16°C and L4s shifted to 25°C overnight before analysis. TH66 (EBP-2::GFP) was maintained at 20°C and L4s were shifted to 25°C for both control and RNAi treatment for 30–32 h before imaging.

RNA Interference Treatment

The *rab-11* feeding vector pR*rab-11* was constructed by cloning the full-length *rab-11* cDNA (F53G12.1/yk1108c6) into the feeding vector L4440 and then transformed into HT115 bacteria (Timmons and Fire, 1998). RNA interference (RNAi) experiments were performed as described (Fire *et al.*, 1998; Timmons and Fire, 1998). Fifteen N2 L4 worms were put on each 30-mm plate and fed for at least 44 h at 20°C before analysis. Green fluorescent protein (GFP)-expressing worms were fed for 30–40 h before analysis as they became sterile after 42 h of feeding. To get same amount of RNAs for RNAi against two genes, we constructed double feeding vectors with both genes between the T7 promoter sites of L4440. The double feeding vectors, pR*rab-11&par-2*, pR*rab-11&par-3*, pR*rab-11&gpr-1/2*, pR*rab-11&dnc-2*, pR*rab-11&let-99*, and pR*rab-11&gpb-1* were made by amplifying each individual gene with the SpeI site added to the primer ends. These PCR fragments were inserted into the pR*rab-11* feeding vector cut with the SpeI site. The following cDNAs or genomic DNA were used: *par-2*: coding region from 1 to 1200 base pairs from yK325e4; *par-3*: coding region from 650 to 2030 base pairs from yk552e12; *gpr-1/2*: full-length yk645d1; *dnc-2*: full-length genomic DNA; *let-99*: full-length yk262g2; and *gpb-1*: coding region from 1 to 820 base pairs from yk325g7. Except for *rab-11&par-2* RNAi, all the RNAi experiments were carried out by feeding 10 or 15 N2 L4s at least 40 h before analysis. For *rab-11&par-2* RNAi, double-strand RNA (dsRNA) was produced using the in vitro T7 transcription Kit (Ambion, Austin, TX). 1 mg/ml dsRNA was injected into N2 young adults and analyzed 36 h later. Full-length *rab-11* 3′ untranslated region (UTR) was amplified and cloned into the L4440 vector. Both N2 and WH347 (RAB-11::GFP) strains were fed at the same time for at least 40 h before imaging or counting dead embryos. The *zyg-9* feeding vector was from Ahringer's feeding library (Kamath *et al.*, 2003).

Live Imaging

Because *rab-11(RNAi)* embryos were sensitive to pressure and osmotic strength (data not shown), embryos were mounted in a hanging-drop blastomere culture medium (Shelton and Bowerman, 1996) for imaging. Worms were cut open in 3 μl blastomere culture medium on the coverslip. A slide with a circle of Vaseline was then pressed onto the coverslip to form a sealed chamber. Four-dimensional Nomarski imaging was performed as described previously (Skop and White, 1998). We used a Nikon Optiphot-2 upright microscope with a Nikon PlanApo 60 × 1.4 NA differential interference contrast (DIC) lens (Melville, NY) and a Hamamatsu C2400 CCD cameras (Hamamatsu Photonics, Hamamatsu City, Japan) or a Nikon Diaphot300 inverted microscope with a 60 × 1.4 NA DIC lens (Melville, NY) and a Sony XC-75 CCD camera (Tokyo, Japan). All GFP images were collected using multiphoton excitation on an optical workstation (Wokosin *et al.*, 2003), which consists of a Nikon Eclipse TE300DV inverted microscope with a Nikon Super Fluor 100 × 1.3 NA lens. The excitation source is a Ti:sapphire laser (Spectra Physics, Mountain View, CA) tuned to 890 nm. The detector is a high quantum efficiency Hamamatsu H7422-40 detector. Except for EBP-2::GFP, images were collected at 512 × 512-pixel resolution at 4.5-s intervals and analyzed with ImageJ v. 1.34s (http://rsb.info.nih.gov/ij/). Images for TH66 (EBP-2::GFP) were collected at 256 × 256-pixel resolution at 0.89-s interval with room temperature at 18°C. The posterior part of the embryos was zoomed in for a better visualization.

Immunohistochemistry

rab-11(RNAi) and WT worms were cut open in blastomere culture medium. Embryos labeled for membrane structures (anti-RAB-11 and anti-HDEL) were prepared as previously described with slight modification (Gonczy *et al.*, 1999b). Fifteen worms were cut open in 15 μl H_2O on a subbed slide. An 18-mm coverslip was placed onto the drop and excess fluid was wicked away with 3MM Whatman paper (Clifton, NJ). The slides were frozen on a metal block in a −80°C freezer for 5 min. After removing the coverslips, the slides were fixed in 100% methanol at −20°C for 15 min. Slides were rehydrated in 1× phosphate-buffered saline (PBS) for 5 min and incubated with 50 μl of primary antibody in PBS for 45 min at room temperature. After the incubation, slides were washed for 5 min in PBT (PBS-0.05% Tween 20), 5 min in PBS, and incubated as described above for 45 min with the secondary antibodies. Slides were washed twice with PBS for 5 min before mounting in 7 μl mounting media (Vectashield; Vector Laboratories, Burlingame, CA). Embryos labeled with the anti-ZYG-8 antibody were fixed in 100% methanol at −20°C for 1 min (P. Gonczy, personal communication). All other antibody labeling was performed using another published protocol (Skop and White, 1998). Staining of WT and *rab-11(RNAi)* embryos was carried out under the same conditions for each antibody. Antibodies were diluted as follows: DM1, mouse anti-α-tubulin, 1:100 (Sigma, St. Louis, MO); rabbit anti-PIE-1, 1:100; rabbit anti-GPR-1/2, 1:200; rabbit anti-ZYG-8, 1:200; rabbit anti-PAR-2 (e3), 1:5; and mouse anti-PAR-3 (P4A1), 1:5 (Developmental Studies Hybridoma Bank, University of Iowa, Iowa City, IA); mouse anti-HDEL, 1:20; rabbit anti-RAB-11, 1:200; and rabbit anti-ZYG-9, 1:40. Secondary antibodies were as follows: goat anti-mouse Alexa 568, 1:200 and goat anti-rabbit Alexa 488, 1:200 (Molecular Probes, Eugene, OR). DNA was labeled using Topro3 (1 mM, 1:500; Molecular Probes, Eugene, OR) and DAPI (1.5 μg/ml, Vectashield). Slides were viewed on a Bio-Rad MRC1024 confocal microscope (Hercules, CA); instrument settings were the same for both WT and experimental embryos within each staining procedure. Images were prepared for publication with Adobe Photoshop (version 8.0, San Jose, CA).

Measure MT Dynamics in rab-11(RNAi) and zyg-8(b235) Embryos

MT length during metaphase in fixed WT, *zyg-8(b235)* and *rab-11(RNAi)* embryos labeled with the anti-α-tubulin antibody was measured as previously described (Gonczy *et al.*, 2001). Namely, the three longest MTs projecting toward the anterior cortex in one optical section from each of five embryos were chosen to measure their length. "MT-cortex gap" refers to the mean distance between the anterior cortex and the plus ends of the longest astral MTs. The posterior astral MTs were adjacent to the posterior cortex in both WT and *rab-11(RNAi)* embryos. The MT growth rate and nucleation rate in *rab-11(RNAi)* embryos were calculated as described (Srayko *et al.*, 2005). Because of the violent movements of both centrosomes during anaphase in *rab-11(RNAi)* embryos, all the measurements were performed with the metaphase MTs and centrosomes. Tracking of EBP-2::GFP was performed manually in ImageJ v. 1.34s. Because some portion of the astral MTs were attached by extra chromosomes because of the polar body extrusion defect, these MTs

no longer underwent active growing in *rab-11(RNAi)* embryos. To make more accurate measurements, a one-quarter circle (instead of a half-circle) was drawn 3.8 μm away from the posterior centrosomes to calculate the MT nucleation rate in movies of 100 frames (89 s). ImageJ v. 1.34s was used to generate the kymograph. The same 89-s movies were also projected into a single image using ImageJ v. 1.34s to reveal the paths of many EBP-2::GFP dots. Student's *t* test with two-tailed unequal variance was used to determine whether the differences of the MT length, MT growth, and nucleation rate between WT and *rab-11(RNAi)* embryos were statistically significant.

RAB-11::GFP

Full-length RAB-11 was amplified from genomic DNA and cloned into the plasmid pFJ1.1 (Squirrell *et al.*, 2006). The plasmid was then bombarded into *unc-119* worms as described (Praitis *et al.*, 2001). Worms were allowed to grow for at least 2 wk. The rescued worms were examined for GFP expression.

Drug Treatments

Nocodazole treatment was carried out as described (Encalada *et al.*, 2005). β-tubulin::GFP or WT worms were cut open on the gasket slide in 5 μl 50 μg/ml to 100 μg/ml nocodazole (Invitrogen, Carlsbad, CA) in egg buffer (Skop and White, 1998). The same dilution of DMSO was used as a control. The coverslip was immediately put on the top of the gasket slide and sealed with petroleum jelly. Embryos undergoing pronuclear migration or centration were imaged either on the multiphoton workstation (β-tubulin::GFP) or with Nomarski optics (N2 embryos). BFA (Invitrogen) treatment was carried out by soaking young embryos, before eggshell formation (usually during meiosis II) in hanging drops containing 150 μg/ml BFA diluted in egg buffer. The same dilution of DMSO was used as control.

Supplemental Data

Supplemental Data including Figures S1 and S2, Tables S1 and S2, and Supplemental Videos are available online.

RESULTS

rab-11(RNAi) Embryos Exhibit Spindle Alignment Defects

It has been previously reported that partial knockdown of RAB-11 by RNAi causes cytokinesis failure (Skop *et al.*, 2001). We found that prolonged RNAi treatment (>44 h) also caused additional abnormalities evident during the first cell cycle, including osmotic sensitivity, failure to extrude polar bodies (52%, n = 23), no or minimal pseudocleavage (83%, n = 12), and failure of the centrosomal-nuclear complex to migrate to the center of the embryos (57%, n = 23). Most strikingly, the P0 spindle failed to rotate to the A-P axis (the angle of the spindle to the A-P axis was 45–90°; 73.9%, n = 23), and the spindle exhibited abnormal displacement during anaphase (100%, n = 23). In WT embryos, the anaphase spindle elongates and moves smoothly toward posterior, with a slight rocking of the posterior centrosome (Figures 1A and 3A; Video 1). By contrast, during the metaphase to anaphase transition, we found that the mitotic spindle underwent violent movements in 82.6% of the *rab-11(RNAi)* embryos (n = 23): the spindle migrated to the posterior pole and then rebounded to the A-P axis (Figures 1B and 3B; Video 2, top). In the remaining embryos (17.4%), both centrosomes rocked extensively and the spindle was displaced further toward the posterior pole (see Figure 3C; Video 2, bottom). The violent spindle movements are specific to RAB-11 depletion, because disruption of other RAB genes (Table S1), known endosome regulators such as RME-1 (Grant *et al.*, 2001) or other osmotic sensitive mutants such as *pod-1* and *pod-2* (Tagawa *et al.*, 2001) did not exhibit similar phenotypes.

Polarity Cues Are Partially Defective in rab-11(RNAi) Embryos

In WT embryos, PAR-2 and -3 occupy mutually exclusive cortical domains, with the smaller PAR-2 domain posterior and the larger PAR -3 domain anterior (Etemad-Moghadam *et al.*, 1995; Boyd *et al.*, 1996; Figure 2, A, C, E, G, and I). When RAB-11 was depleted by RNAi, the PAR-2 domain

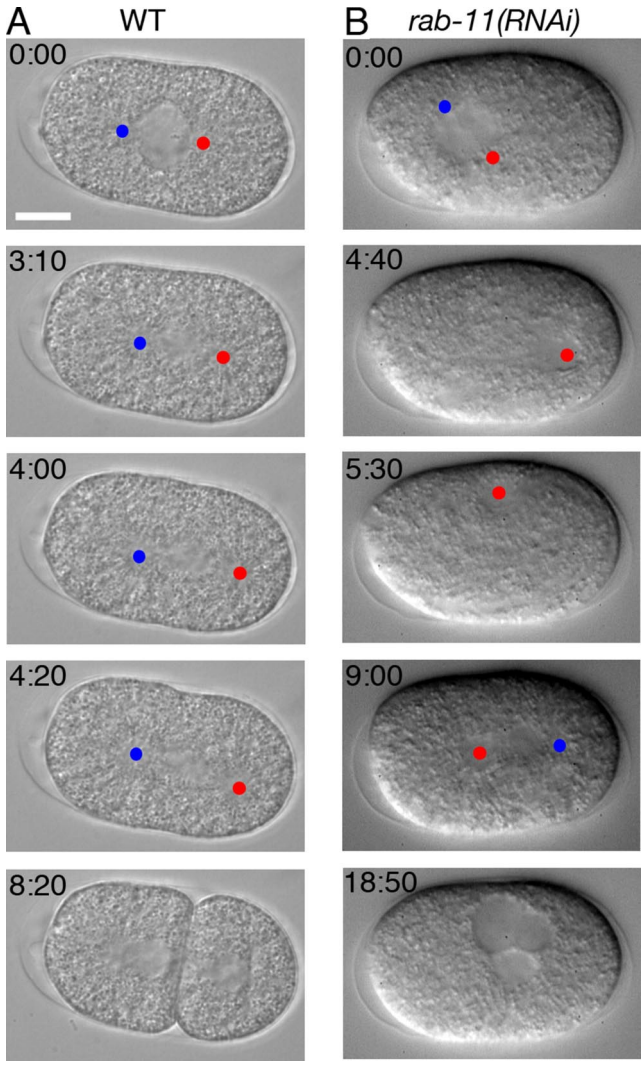

Figure 1. *rab-11(RNAi)* embryos undergo violent spindle movements during one-cell anaphase. Time-lapse differential interference contrast (DIC) microscopy recordings of the first cell division of WT embryo (A, Video 1), and *rab-11(RNAi)* embryo (B, Video 2) after 44 h of feeding from prometaphase (t = 0) to the end of the first division. Blue dots, anterior centrosomes; red dots, posterior centrosomes. In the *rab-11(RNAi)* embryo, the P0 spindle did not align along the anterior-posterior axis of polarity and the posteriorly positioned centrosome (labeled with red dot) ended up in an anterior location at the end of anaphase due to the violent spindle movements. The anterior positioned centrosome was out of focus at some time points. Cytokinesis of the first division failed to complete in the *rab-11(RNAi)* embryo. Scale bar, 10 μm.

was reduced in size, whereas the boundary of PAR-3 expanded further to the posterior (Figure 2, B, D, F, H, and I). In some cases, the PAR-3 domain ectopically localized to the posterior cortex (50%, n = 6). Similar observations were seen with live images of PAR-2::GFP– and PAR-6::GFP–expressing embryos (data not shown). In some embryos the two domains partially overlapped as shown by immunofluorescence staining (Figure 2H). This ectopic localization of PARs resembles that seen in *par-4*– and *-5*–deficient embryos, although these do not exhibit violent anaphase spindle displacement (Hung and Kemphues, 1999; Watts *et al.*, 2000; Morton *et al.*, 2002). Although the boundary of PAR-2 and -3 was shifted toward the posterior, the anterior-posterior

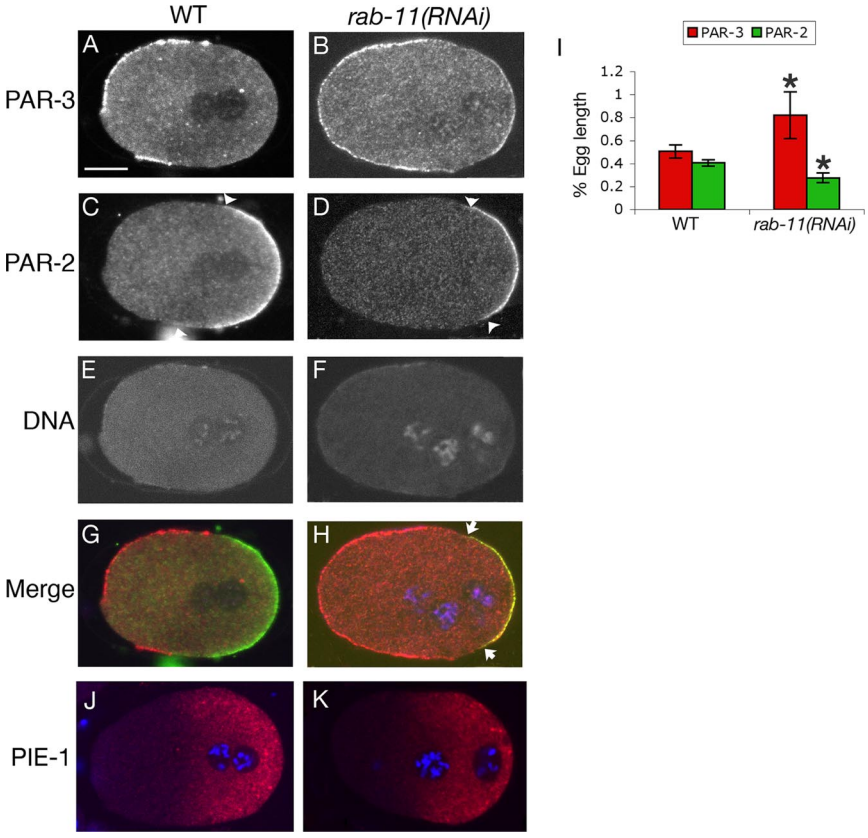

Figure 2. Polarity defects in *rab-11(RNAi)* embryos. WT (A, C, E, and G) and *rab-11(RNAi)* (B, D, F, and H) one-cell embryos stained with anti-PAR-3 (A and B), anti-PAR-2 (C and D) antibodies and Topro3 (E and F) to reveal DNA. Arrowheads mark the boundary of the PAR-2 domain. In the merged images (G and H), PAR-3 is red, PAR-2 is green, and DNA is blue. Arrows indicate the boundary of the overlapping region of PAR-2 and -3 in *rab-11(RNAi)* embryos. Note the extra pronucleus indicating the polar body was not extruded in the *rab-11(RNAi)* embryo. (I) Quantification of the egg length of PAR-2 and -3 domains before pronuclear centration in WT and *rab-11(RNAi)* embryos. n = 6 embryos for each measurement. Error bars, SD. Statistically significant difference between WT and *rab-11(RNAi)* embryos; *$p < 0.05$; Student's *t* test, two-tailed unequal variance. For PAR-2, $p = 0.00016$; PAR-3, $p = 0.011$. (J and K) Immunofluorescence staining of PIE-1 (red) in WT (J) and *rab-11(RNAi)* (K) embryos during pronuclear migration. DNA (blue) is labeled with Topro3. Scale bar, 10 μm.

polarity was not totally abolished, as the germline factor PIE-1 still segregated normally to the posterior (Figure 2, J and K).

In WT embryos, GPR-1/2 is enriched at the posterior cortex in response to PAR-2 and -3 localization (Colombo *et al.*, 2003; Gotta *et al.*, 2003; Figure 3J). We found the size of the cortical region of GPR-1/2 was reduced in *rab-11(RNAi)* embryos between the end of prophase and early anaphase (n = 21; Figure 3K). This defect was probably a result of the posterior shift of the PAR-2 and -3 boundary in *rab-11(RNAi)* embryos (Figure 2). Nevertheless, the level of GPR-1/2 was not more highly enriched on the posterior cortex than in the WT embryos. This observation suggests that the polarity defect may not cause elevated level of GPR-1/2 on the posterior cortex and therefore is unlikely to explain the violent spindle movements.

Violent Spindle Movements in rab-11(RNAi) Embryos Are Subjected to Gα/GPR-1/2 Regulation

It is known that Gα and its upstream activator GPR-1/2 are the major force regulators for anaphase spindle displacement in the one-cell *C. elegans* embryo (Cowan and Hyman, 2004a). Because *rab-11(RNAi)* embryos exhibit violent spindle movements, we first examined whether Gα/GPR-1/2 regulation was altered in *rab-11(RNAi)* embryos. When we used RNAi to deplete PAR-3, LET-99, or GPB-1, proteins that function to down-regulate Gα/GPR-1/2 activity (Colombo *et al.*, 2003; Gotta *et al.*, 2003; Tsou *et al.*, 2003), in *rab-11(RNAi)* embryos the violent spindle movements became more dramatic (Figure 3, D–F). Specifically, in *par-3; rab-11(RNAi)* embryos, the spindle still underwent violent movements but remained positioned in the center of the embryo instead of being pulled to the posterior (100%, n = 11; Figure 3D; Video 3, top), indicating that strong pulling forces were distributed around the entire cell. In *rab-11;let-99(RNAi)* and *rab-11;gpb-1(RNAi)* embryos, the centrosomal-nuclear complex, as well as the mitotic spindle, exhibited even more violent movements than depleting RAB-11 by itself. These violent movements commenced from the time of pronuclear centration until the embryo reached anaphase (*rab-11;let-99(RNAi)*: 36.4%, n = 11; *rab-11;gpb-1(RNAi)*: 18.2%, n = 11; Figure 3, E and F; Video 4). Conversely, the violent spindle movements in *rab-11(RNAi)* embryos were suppressed when G_{α} activity was down-regulated, such as in *rab-11;par-2(RNAi)* embryos (91.7%, n = 12; Figure 3G; Video 3, bottom; Colombo *et al.*, 2003; Gotta *et al.*, 2003), as well as in *rab-11;gpr-1/2 (RNAi)* embryos (100%, n = 10; Figure 3H; Video 5, top). Because Gα/GPR-1/2 can be both up- and down-regulated, resulting in a concomitant change in the violence of spindle movements, it is unlikely that constitutively active Gα/GPR-1/2 activity is the cause of the excessive spindle movement in *rab-11(RNAi)* embryos. Furthermore, our immunofluorescence staining with anti-GPR-1/2 antibody also suggests that the Gα activity was not up-regulated in *rab-11(RNAi)* embryos (Figure 3, J and K). We also found that the violent spindle movements required the activity of dynein-dynactin (n = 16; Figure 3I), suggesting they are the downstream targets of Gα/GPR-1/2. These observations indicate a correlation between Gα/GPR-1/2 activity and the extent of the violent spindle movements and that *rab-11(RNAi)* did not disrupt the interactions among the regulators of the normal anaphase spindle displacement.

MT Dynamics during Metaphase Are Altered in rab-11(RNAi) Embryos

Because MT dynamics are likely to play a crucial role in spindle orientation and movements, we examined the MTs

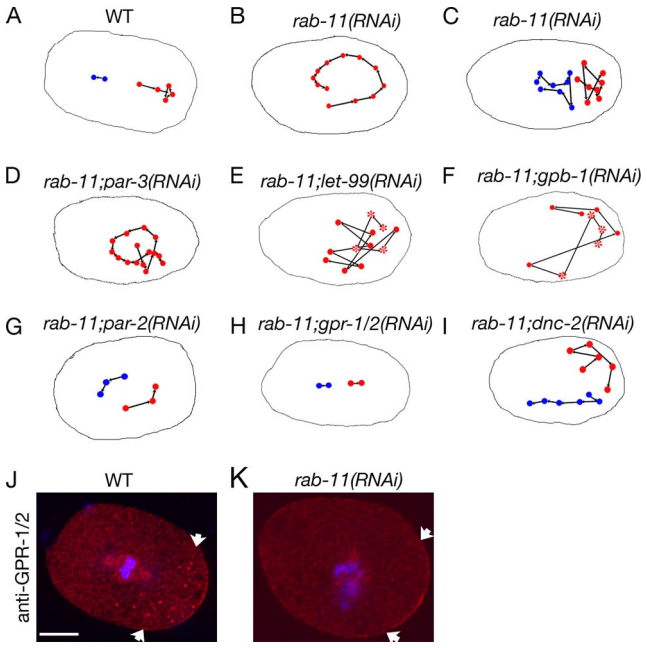

Figure 3. Gα/GPR-1/2 activity may not be up-regulated in *rab-11(RNAi)* embryos. Schematic representations of the movements of one or both centrosomes in WT (A, Video 1), *rab-11(RNAi)* (B and C, Video 2), *rab-11; par-3(RNAi)* (D, Video 3, top), *rab-11; let-99(RNAi)* (E, Video 4, top), *rab-11; gpb-1(RNAi)* (F, Video 4, bottom), *rab-11; par-2(RNAi)* (G, Video 3, bottom), *rab-11; gpr-1/2(RNAi)* (H, Video 5, top), and *rab-11; dnc-2(RNAi)* embryo (I, Video 5, bottom). Each drawing is from a single representative embryo. These trajectories describe the path of centrosome movement from prometaphase to the end of anaphase (dots). The dots are not at the same time intervals. For *rab-11; let-99(RNAi)* and *rab-11; gpb-1(RNAi)* embryos (E and F), because the violent movements of the centrosomes begin before that observed in *rab-11(RNAi)*, the traces of movements start from pronuclear centration (asterisks). In embryos whose spindles underwent violent movements, only the posterior centrosomes are shown as the anterior centrosomes were frequently out of the plane of focus. In the *rab-11; par-2(RNAi)* (G) and *rab-11; dnc-2(RNAi)* (I) embryos, the P0 spindles first set up perpendicular to the longitudinal axis. In *rab-11; dnc-2(RNAi)* embryo, the spindle failed to centrate due to disruption of DNC-2 activity. During anaphase, the spindles elongated and flipped to the longitudinal axis due to the constraints of the eggshell. (J and K) Immunofluorescence staining of GPR-1/2 (red) in WT (J) and *rab-11(RNAi)* (K) embryos during one-cell metaphase. DNA (blue) is labeled with Topro3. Arrows delineate regions of GPR-1/2 enrichment at posterior cortex. In the *rab-11(RNAi)* embryo, the P0 spindle did not rotate and the chromosomes did not align properly along the metaphase plate. Immunolabeled *rab-11(RNAi)* embryos are larger because they are pressure sensitive and flattened more than WT embryos during fixation. Scale bar, 10 μm.

in *rab-11(RNAi)* embryos. Immunofluorescence staining of MTs and imaging of EBP-2::GFP (the worm EB1 homolog that labels the growing MT plus ends) revealed that astral MT organization was altered in *rab-11(RNAi)* embryos. Although the anaphase MTs were normal in *rab-11(RNAi)* embryos, during metaphase aspects of MT dynamics, such as the distance between the plus ends of the MTs and the anterior cortex, MT growth, and nucleation rates (Table 1 and Figure 4, B and E), were altered compared with WT. During metaphase the distance between MT plus ends and the cortex was significantly greater in *rab-11(RNAi)* embryos than WT, probably because of the reduced MT length: 14.0 ± 1.6 μm in *rab-11(RNAi)* embryos compared with 22.1 ± 4.4 μm in WT ($p < 0.001$), although at anaphase, the MT ends contacted the cortex in both cases (Table 1). In addition, fewer growing astral MTs reached to the cortex during metaphase in *rab-11(RNAi)* embryos (n = 3/3) than in WT (Figure 4H, Video 6), suggesting the catastrophe rate may also be higher in *rab-11(RNAi)* embryos, although this rate cannot be measured directly using the EBP-2::GFP marker. This observation indicates that the inability of MT to reach the cortex in metaphase in these *rab-11(RNAi)* embryos may result from both slow growth and increased MT depolymerization.

It has been reported that embryos carrying a mutation in *zyg-8*, a Doublecortin-related kinase, exhibit similar exaggerated anaphase spindle displacement as observed in *rab-11(RNAi)* embryos (Gonczy *et al.*, 2001). In *zyg-8(t1650)* embryos, the length of the metaphase astral MTs is normal, whereas the anaphase MTs are shorter compared with those in WT embryos (Gonczy *et al.*, 2001). Similarly, we found that the distance between the plus ends of the MTs and the cortex in *zyg-8(b235)* embryos resembles WT, but at anaphase a gap remains between the MT ends and the cortex. By contrast, in both WT and *rab-11(RNAi)* embryos the MT ends touch the cortex at anaphase (Figure 4, D and E, Table 1). In some *zyg-8(b235)* embryos, the spindle sets up in the posterior, perpendicular to the anterior-posterior axis (Figure 4F). In these embryos, the distance between the MTs and the cortex at anaphase is even more extensive (18.9 ± 1.6 μm). Furthermore, it has been shown that MT nucleation rate at metaphase is 36% higher in *zyg-8(t1650)* embryos than in WT (Srayko *et al.*, 2005), whereas in *rab-11(RNAi)* embryos the MT nucleation rate is reduced at metaphase, compared with WT (Table 1). Therefore, the effects of RAB-11 levels on MT length are unlikely to be mediated through ZYG-8 because MT dynamics differ between *rab-11(RNAi)* and *zyg-8* mutant embryos. Additionally, ZYG-8 localization to the spindle and spindle poles was not affected in *rab-11(RNAi)* embryos (Figure 4, I and J). These observations suggest that the length of the astral MTs is regulated by different mechanisms during the cell cycle. Indeed, it has been shown that, at least for the spindle MTs, the turnover rate is faster during prometaphase than anaphase in *C. elegans* one-cell embryos (Labbe *et al.*, 2004).

We investigated next whether short metaphase MTs were sufficient to drive the violent spindle movements seen in the *rab-11(RNAi)* embryos by using the MT-depolymerizing drug nocodazole. The nocodazole dose and time of application were adjusted such that astral MTs in treated embryos were shortened during metaphase, yet the drug effect wore off during anaphase so that the astral MTs resumed elongation. We found that although the spindle movements in control embryos were normal (Figure 5A; Video 7), in embryos treated with nocodazole in this manner, the spindles underwent "*rab-11*-like" movements: either moving to the posterior (n = 3/7) or with both centrosomes rocking extensively (n = 4/7; Figure 5, B and C; Videos 8 and 9). This observation further supports the notion that a polarity defect in *rab-11(RNAi)* embryos does not necessarily contribute to the violent spindle movements because nocodazole treatment does not affect polarity (Cowan and Hyman, 2004b) yet is sufficient to generate the violent spindle movements.

Metaphase ER Morphology Is Disrupted in rab-11(RNAi) Embryos

To understand further the role of RAB-11 in spindle alignment, we generated transgenic worms expressing RAB-11::GFP in the embryo under the control of the *pie-1* promoter together with its UTRs. RNAi against the *rab-11*

Table 1. *rab-11(RNAi)* and *zyg-8(b235)* embryos exhibit different defects in MT dynamics

	MT-cortex gap		MT dynamics	
	Metaphase	Anaphase	Metaphase MT growth rate	Metaphase MT nucleation rate
N2	2.8 ± 1.4 μm	Adjacent	0.72 ± 0.04 μm/s	102 ± 6
rab-11(RNAi)	17.2 ± 5.1 μm[a]	Adjacent	0.54 ± 0.06 μm/s[a,b]	67 ± 7[a]
zyg-8(b235)	3.3 ± 1.5 μm	8.8 ± 2.9 μm		

Measurements of MT dynamics in *rab-11(RNAi)* embryos are described in *Methods and Materials.* "MT-cortex gap" refers to the mean distance between the anterior cortex and the plus ends of the longest astral MTs in a single optical section in embryos in which the spindle is essentially parallel to the anterior-posterior axis.

[a] Statistically significant difference from WT (Student's *t* test with two-tailed unequal variance).

[b] EBP-2::GFP worms became sterile after 32 h of *rab-11* RNAi treatment before the embryos showed the severe spindle alignment defects. This growth rate may be even slower with prolonged RNAi treatment using wild-type N2 embryos (>44 h of *rab-11* RNAi), as we observed an inverse relationship between the duration of *rab-11* RNAi treatment and MT length in embryos labeled with tubulin antibody (data not shown).

3′UTR was carried out to determine whether the GFP fusion protein was functional. All embryos lacking the transgene failed cytokinesis at the first division (n = 6), whereas embryos expressing the RAB-11::GFP completed early cell divisions normally (n = 6), although they died at a later stage. The late lethality is probably due to loss of RAB-11::GFP expression when the *pie-1* promoter shuts down in older embryos (Mello *et al.*, 1996). The GFP signal localized to cytoplasmic puncta, around centrosomes, and at the periphery of the mitotic spindle (Figure 6, A and B). We also found RAB-11::GFP enriched at the spindle midbody, consistent with observations in mammalian cells (Wilson *et al.*, 2005; data not shown). Indirect immunofluorescence labeling with an antibody raised against *C. elegans* RAB-11 (Poteryaev *et al.*, 2007) confirmed the GFP localization. Furthermore, these observations revealed a more elaborate cytoplasmic structure not obvious in the GFP strain (Figure 6, C and D). By costaining with an ER antibody (anti-HDEL), we were surprised to find RAB-11 (i.e., putative recycling endosomes) colocalized extensively with ER, although there were regions unique to each organelle (Figure 6, C–I).

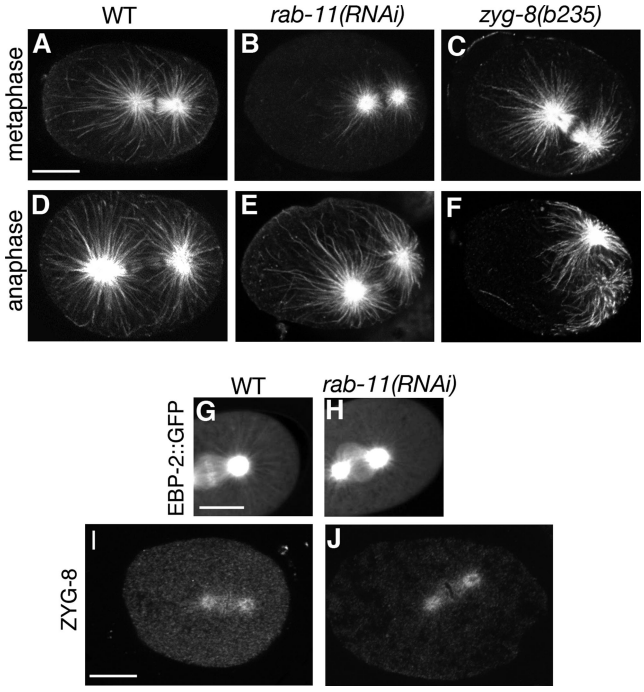

Figure 4. *rab-11(RNAi)* and *zyg-8(b235)* embryos exhibit different MT length defects during one-cell division. (A–C) Metaphase MTs stained with anti-α-tubulin antibody in WT (A), *rab-11(RNAi)* (B), and *zyg-8(b235*) (C) embryos. (D--F) Anaphase MTs stained with anti-α-tubulin antibody in WT (D), *rab-11(RNAi)* (E), and *zyg-8(b235)* (F) embryos. (G and H) Projections of 100-frame EBP-2::GFP movies (89 s in length) in WT (G, Video 6, left) and *rab-11(RNAi)* (H, Video 6, right) embryos during metaphase (see *Materials and Methods*). Very few MTs were seen to grow out to the cortex in the *rab-11(RNAi)* embryos (H). Notice that EBP-2::GFP accumulation at the kinetochore–MT interface was also reduced in *rab-11(RNAi)* embryos. The significance of this defect is not known. (I and J) Immunofluorescence staining of ZYG-8 in WT (I) and *rab-11(RNAi)* (J) embryos. ZYG-8 localization to the spindle and centrosomes was normal in the *rab-11(RNAi)* embryos, although the cytoplasmic staining seemed to be reduced in *rab-11(RNAi)* embryo. Scale bar, 10 μm.

Because of the overlap between RAB-11 and ER structures, we examined ER morphology in *rab-11(RNAi)* embryos by both immunofluorescence staining with anti-HDEL antibody as well as in live embryos expressing an ER marker, SP12::GFP. We found in both cases that although the perispindle ER was still normal, the ER formed large aggregates throughout the cytoplasm in metaphase (Figure 7, C and H). During anaphase, the ER was still able to undergo morphological transitions from reticulate to dispersed structures as seen in the WT embryos (Poteryaev *et al.*, 2005), and the large aggregates disappeared at the end of anaphase (Figure 7, D and H). Similarly, we found that the ER formed large aggregates during metaphase in *zyg-8(b235)* embryos (n = 5/5); Figure 7E). However, unlike in *rab-11(RNAi)* embryos, these aggregates persisted through anaphase (n = 4/4; Figure 7F), possibly accounting for the observed differences in MT length between these two cases.

ER Morphology in Embryos Where Spindle Alignment Genes Are Affected

How the ER influences spindle alignment in *C. elegans* early embryos is not well understood. Representative mutants, gene knockdowns or drug treatments that affect ER morphology, spindle alignment, or both are summarized in Table 2. Disrupting two *C. elegans* ER proteins OOC-3 and -5 as well as applying BFA to young embryos all led to large ER aggregates during metaphase that persisted until anaphase

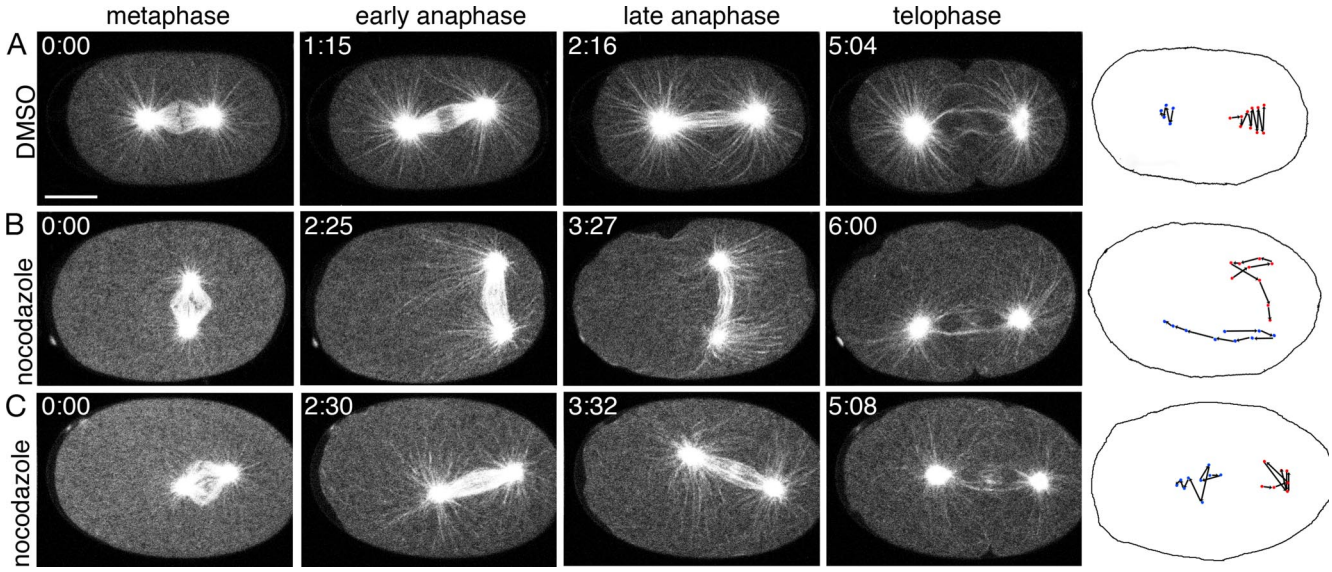

Figure 5. Nocodazole treatment can phenocopy the violent spindle movements in *rab-11(RNAi)* embryos. Multiphoton time series of embryos expressing β-tubulin::GFP show the following developmental stages: metaphase, early anaphase, late anaphase, and telophase. (A) β-tubulin::GFP embryos treated with the same dilution of DMSO (Video 7). (B and C) β-tubulin::GFP embryos treated with 50 μg/ml nocodazole during pronuclear migration or centration (Videos 8 and 9). Note that the metaphase MTs were shortened by nocodazole, but they resumed elongation during anaphase. Centrosomal positions that best describe the trace of the movements from metaphase to telophase are shown in the schematic drawings (blue dots, anterior centrosomes; red dots, posterior centrosomes; dots are not at the same time intervals). Scale bar, 10 μm.

(Figure 8, A and B; Table 2; Basham and Rose, 2001; Poteryaev *et al.*, 2005). Although the disrupted ER morphologies were similar, their associated spindle alignment defects were quite different: in *ooc-3(mn241)* and *ooc-5(it145)* mutant embryos; both P0 and P1 spindles fail to align along the A-P axis (Basham and Rose, 1999; Pichler *et al.*, 2000; Basham and Rose, 2001), whereas in BFA-treated embryos the nuclear-centrosomal complex rocked during pronuclear centration (100%, n = 14; Figure 8, I and J; Video10). None of these conditions affected the length of MTs (Basham and Rose, 1999, 2001; Pichler *et al.*, 2000; Figure 8, C and D; data not shown) as seen in *rab-11(RNAi*) embryos, suggesting that the ER may influence spindle alignment by multiple mechanisms. On the other hand, some genes that are required for

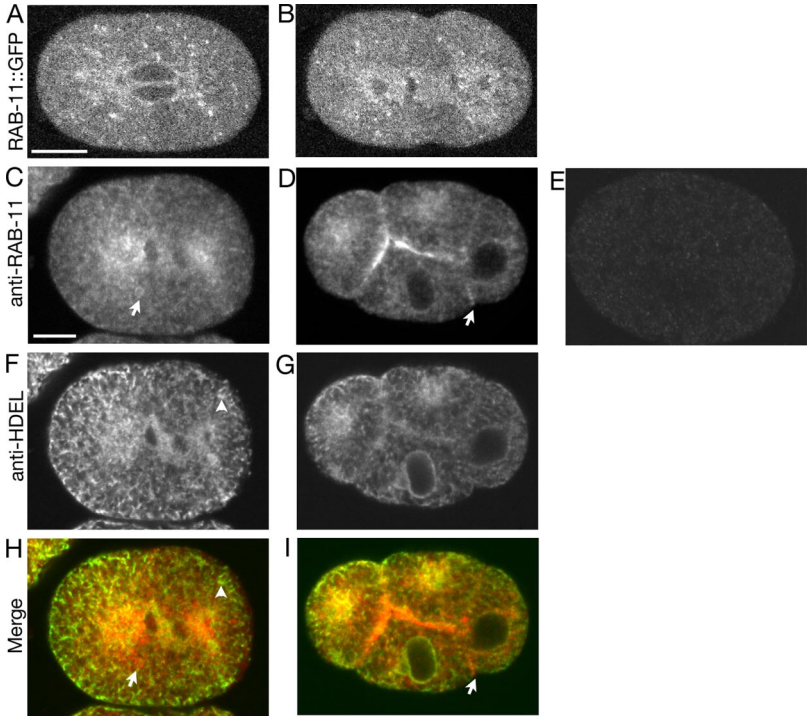

Figure 6. RAB-11 colocalizes extensively with the ER. Metaphase (A) and anaphase (B) localization of RAB-11::GFP. One-cell anaphase embryo labeled with anti-RAB-11 (C), anti-HDEL (F), and merged (H). Four-cell embryo with ABa and ABp at anaphase, P2 and EMS at metaphase labeled with anti-RAB-11 (D), anti-HDEL (G), and merged (I). Arrow points to a structure unique to anti-RAB-11 labeling, and arrowhead to a structure unique to anti-HDEL labeling. In *rab-11(RNAi)* embryo (E), the anti-RAB-11 labeling is greatly reduced. Scale bar, 10 μm.

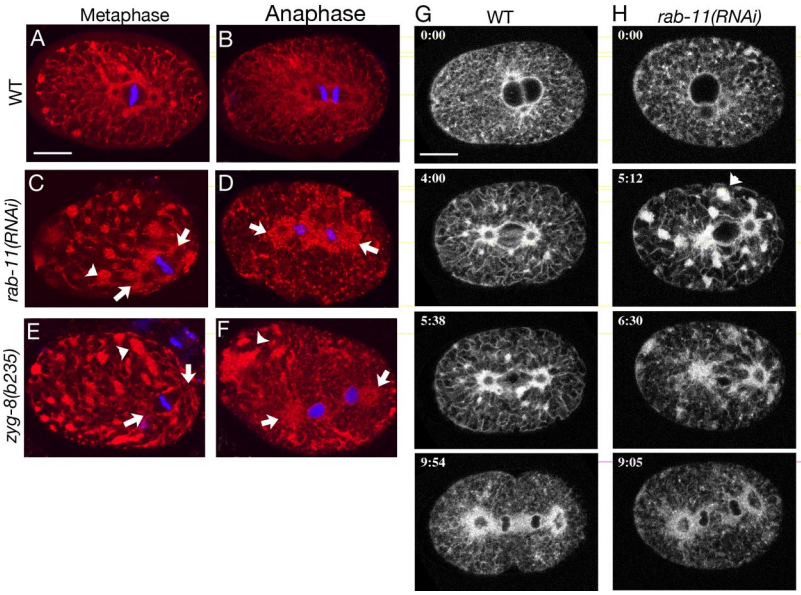

Figure 7. Metaphase ER morphology is disrupted in *rab-11(RNAi)* embryos. Immunofluorescence staining of the ER (anti-HDEL, red) and Topro3 staining of DNA (blue) in metaphase and anaphase WT embryos (A and B), *rab-11(RNAi)* embryo (C and D), and *zyg-8(b235)* mutant embryos (E and F). Arrows mark the positions of the mitotic spindle poles. Arrowhead shows one of the ER clumps. (G and H) Multiphoton time series of embryos expressing SP12::GFP show the following developmental stages: prometaphase (t = 0), metaphase, early anaphase, and late anaphase. Arrowhead shows one of the ER clumps in metaphase. Scale bar, 10 μm.

normal ER morphology, such as *car-1,* may not be required for spindle alignment because, in *car-1* depleted embryos, although violent spindle rocking occurs during anaphase as the spindle midzone breaks, the initial spindle rotation and spindle alignment looks similar to WT (Squirrell *et al.,* 2006; Table 2), indicating that disrupting ER organization does not necessarily lead to spindle alignment defect.

We next examined the ER morphologies of embryos in which the spindle alignment regulators had been suppressed by RNAi. These proteins normally act by either modulating the interactions between the cortex and the astral MTs, such as the trimetric G proteins (Labbe *et al.,* 2003) and LET-99 (Tsou *et al.,* 2002; Tsou *et al.,* 2003) or affecting the MT length, such as ZYG-9 (Matthews *et al.,* 1998; Gonczy *et al.,* 2001). ER morphology was normal in GPB-1–, GPR-1/2–, and LET-99–depleted embryos (Figure 8, E and F; Table 2). Similar results were obtained in ZYG-9–depleted embryos, which exhibit abnormal MT length independently of the cell cycle (Figure 8, G and H; Table 2).

DISCUSSION

Short Astral MTs at Metaphase Contribute to Violent Spindle Movements during Anaphase

Both *rab-11(RNAi)* and *zyg-8* mutant embryos exhibit violent spindle movements during anaphase in the P0 cell. In *zyg-8(t1650)* animals this violent spindle movement is caused by the failure of astral MT elongation during anaphase (Gonczy *et al.,* 2001), whereas in *rab-11(RNAi)* embryos the lengths of the anaphase astral MTs were normal and the metaphase astral MTs were much shorter compared with those in WT embryos. How do short astral MTs at metaphase cause violent spindle alignment during anaphase?

In WT embryos a posterior pulling force acts on the spindle during late prophase and prometaphase but is balanced by the tethering of astral MTs at the anterior cortex (Labbe *et al.,* 2004; Figure 9A). We propose that the short astral MTs observed during metaphase in *rab-11(RNAi)* embryos cannot be tethered by the anterior cortex; thus the spindle becomes prematurely subjected to the posterior pulling force. This posterior pulling force may be exerted on the spindle by the few astral MTs that do manage to reach to the posterior cortex and can be captured and shortened by the active force generators (e.g., dynein-dynactin; Figure 9B). Indeed, the number of the active force generators that displace the anaphase spindle in the WT embryo may be as few as 50 throughout the embryo, with more being present on the posterior cortex (Grill *et al.,* 2003). We hypothesize that interactions between cortex and the many anterior astral MTs may function to counter the posterior pulling force in normal situations. Both reduction of the astral MT length and number are necessary to reach a certain threshold in order to destabilize the balance and generate the violent spindle movements that we observed. The observation that nocodazole-treated embryos showed a similar range of defects supports this hypothesis.

A model in which RAB-11 acts to regulate metaphase astral MT length, depicted in Figure 9, can also explain the modulations of the violent spindle movements in *rab-11(RNAi)* embryos shown in Figure 3. In particular, when there is elevated cortical GPR-1/2 (thereby producing higher Gα activity), the pulling force from the posterior cortex is enhanced, resulting in more violent spindle movements (Figure 9, C and D). In contrast, reduced cortical localization of GPR-1/2 (Figure 9, E and F) or inactivation of the motor dynein-dynactin (Figure 9G) results in reduced pulling force from the posterior, and the spindle movements are suppressed.

RAB-11 Can Colocalize with and Contribute to the Organization of the ER

Rab11 localizes mainly to the peri-centrosomal region in interphase Chinese hamster ovary (CHO) cells with a lower concentration of puncta distributed throughout the cell (Ullrich *et al.,* 1996), whereas in polarized MDCK cells during mitosis, Rab11 forms diffuse puncta in the cytosol during prophase and then becomes clustered near the spindle poles after metaphase; this spindle pole accumulation increases throughout telophase (Hobdy-Henderson *et al.,* 2003). However, we found that *C. elegans* RAB-11 overlaps with ER extensively and is required for normal ER morphology specifically during metaphase. Although the astral MTs were short during metaphase in *rab-11(RNAi)* embryos, the perturbation in ER morphology that we observed is probably

Table 2. ER morphology by depletion of spindle alignment genes or drug treatment

Genes or drug	ER forms large aggregates during metaphase	Large aggregates persist during anaphase	ER cycles	Spindle alignment defect	Astral MT length defect	Reference
rab-11 RNAi	Yes, throughout the cytoplasm (n = 16, Figure 7H)	No, the large aggregates dispersed (n = 16, Figure 7H)	Yes	Yes, P0 spd rotation defect and violent anaphase spindle movements	Short metaphase astral MTs (n = 27, Figure 4B)	This study
zyg-8 (b235)	Yes, throughout the cytoplasm (n = 5, Figure 7E)	Yes, throughout the cytoplasm (n = 4, Figure 7F)	Yes	Yes, P0 spd rotation and anaphase spindle position defect	Short anaphase astral MTs (n = 11, Figure 4F)	Gonczy *et al.* (2001)
zyg-9 RNAi	No (n = 4, Figure 8G)	No (n = 4, Figure 8H)	Yes	Yes, P0 spd set up transversely at posterior	Short MTs throughout cell cycle	Matthews *et al.* (1998)
let-99 RNAi	No (n = 5/6, Figure 8E)	No (n = 5, Figure 8F)	Yes	Yes, centrosomal-pronuclear complex wobble during centration, P0 and P1 spindle rotation defect	Normal	Rose and Kemphues (1998); Tsou *et al.* (2002, 2003)
gpb-1 RNAi	No (n = 3, data not shown)	No (n = 3, data not shown)	Yes	Yes, centrosomal-pronuclear complex wobble during centration, P0 and P1 spindle rotation defect	Normal	Gotta and Ahringer (2001); Tsou *et al.* (2003)
gpr-1/2 RNAi	No (n = 3, data not shown)	No (n = 3, data not shown)	Yes	No anaphase spindle elongation and displacement	Normal	Colombo *et al.* (2003); Gotta *et al.* (2003)
ooc-3/ooc-5	Yes, throughout the cytoplasm (n = 3, Figure 8A)	Yes, throughout the cytoplasm (n = 3, Figure 8B)	Yes	Yes, P0 and P1 spd fail to align along A-P axis	Normal (n = 3, Figure 8, C and D)	Basham and Rose (1999, 2001); Pichler *et al.* (2000)
BFA	Yes, throughout the cytoplasm	Yes, throughout the cytoplasm	No	Yes, centrosomal-pronuclear complex rock during centration (Figure 8, I and J)	Normal (n = 3, data not shown)	Poteryaev *et al.* (2005), and this study
car-1 RNAi	No, but patchy accumulation or thick strand	patchy accumulation or thick strand persist	Yes	No	Normal	Squirrell *et al.* 2(006)
cdc48 RNAi	Yes, throughout the cytoplasm	Yes, throughout the cytoplasm	No	No	ND	Poteryaev *et al.* (2005), and personal communication
hsp-4 RNAi	Yes, throughout the cytoplasm	Yes, throughout the cytoplasm	No	No	ND	Poteryaev *et al.* (2005), and personal communication

ND, not determined.

not a secondary effect of the MT disruption, as seen in a number of organisms (Voeltz *et al.*, 2002), because disrupting the MT cytoskeleton by nocodazole, *tba-2(RNAi)* (Poteryaev *et al.*, 2005) or *zyg-9(RNAi)* (this work) does not affect the ER morphological changes in *C. elegans* early embryos.

Why Are Astral MTs Shorter in rab-11(RNAi) Embryos than in WT at Metaphase?

One possible explanation is that RAB-11 (possibly in conjunction with its RE binding partner FIP3; see Supplementary Data) is required for delivery of proteins that can modulate MT lengths (such as MT-associated proteins [MAPs]) to astral MTs via the REs. When we examined the localizations of several known MAPs in *C. elegans* early embryos, such as EBP-2, ZYG-8 and -9, and dynactin (DNC-2), none were affected by RAB-11 depletion (Figure 4, H and J, and data not shown); however, some other MAPs may be involved. It is possible that changes in the cortical cytoskeleton contribute to the reduction of the observed MT length. However, we did not observe any significant perturbation in the distribution of cortical myosin before cytokinesis (Supplemental Data).

It may be significant that both astral MT length and ER morphology were affected in *rab-11(RNAi)* embryos predominantly during metaphase. This observation, together with the extensive colocalization between RAB-11 and ER that was seen, suggests that RAB-11 could mediate the cell-cycle–specific regulation of MT length through its effect on

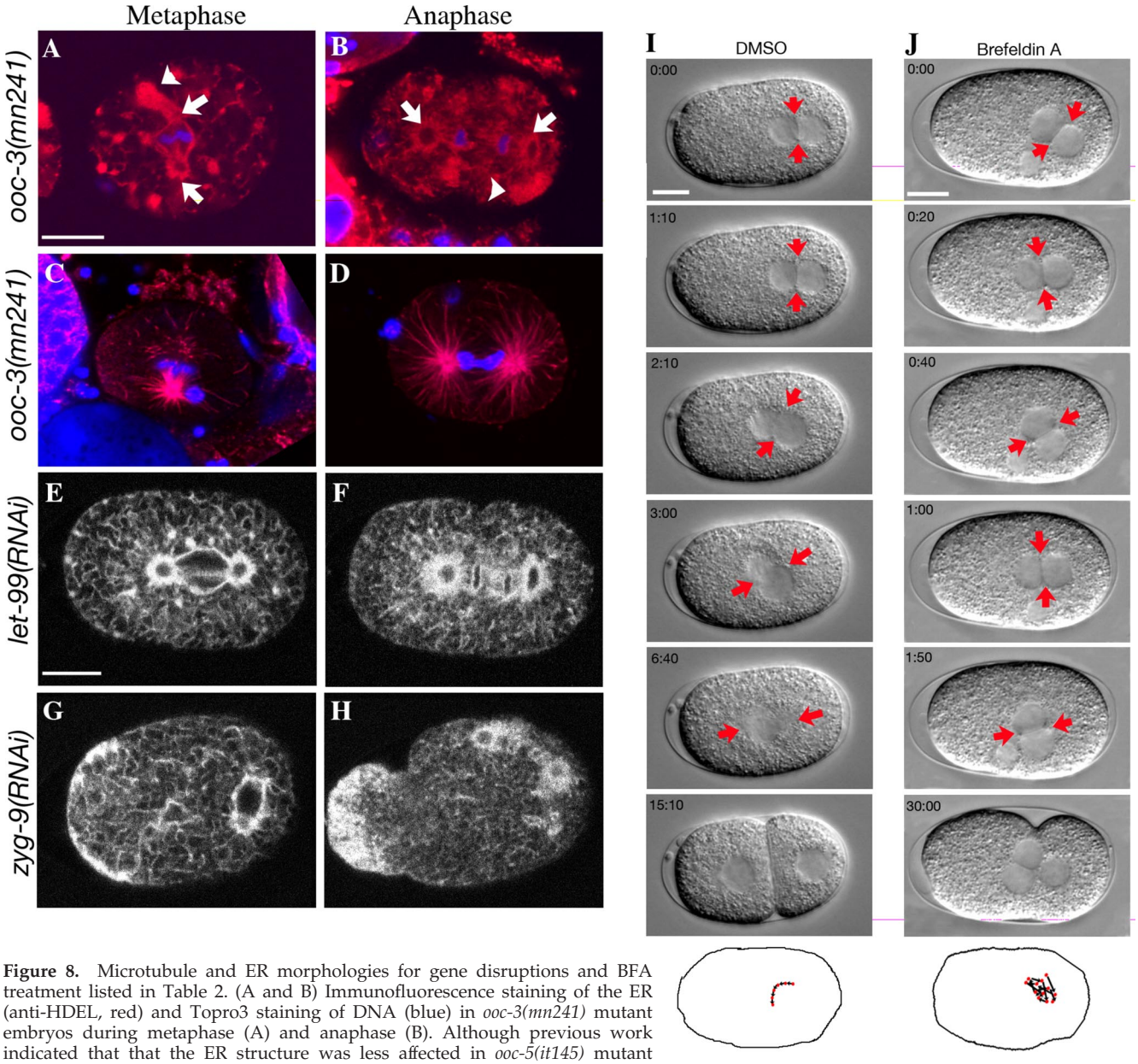

Figure 8. Microtubule and ER morphologies for gene disruptions and BFA treatment listed in Table 2. (A and B) Immunofluorescence staining of the ER (anti-HDEL, red) and Topro3 staining of DNA (blue) in *ooc-3(mn241)* mutant embryos during metaphase (A) and anaphase (B). Although previous work indicated that that the ER structure was less affected in *ooc-5(it145)* mutant embryos than in *ooc-3(mn241)* embryos (Basham and Rose, 2001), we observed a similar defect of ER morphology in these embryos (data not shown). Arrows mark the position of the mitotic spindle poles. Arrowheads show one of the ER clumps. (C and D) Immunofluorescence staining of the microtubules (red) and Topro3 staining of DNA (blue) in *ooc-3(mn241)* mutant embryos during one-cell metaphase (C) and anaphase (D). *ooc-5(it145)* mutant embryos showed similar phenotype (data not shown). *ooc-3(mn241)* and *ooc-5(it145)* mutant embryos are often smaller than the WT embryos (Basham and Rose, 1999). Scale bar, 10 μm. (E and F) SP12::GFP embryos treated with *let-99* RNAi showed that ER morphology was not affected during either metaphase (E) or anaphase (F). (G and H) SP12::GFP embryos treated with *zyg-9* RNAi showed that ER morphology was similar to that observed with nocodazole or *tba-2(RNAi)* treatment (Poteryaev *et al.*, 2005). The accumulation of ER structure at the anterior during anaphase may be due to the exaggerated cytoplasmic flow resulting from short microtubules. (I and J) BFA treatment caused nuclear-centrosomal complex rocking during pronuclear centration. Nomarski images show the centrosome movements during pronuclear centration and the final stage of the first division (the last time point). (I, Video 10, top) WT meiosis II embryos treated with same dilution of DMSO as control (n = 15). (J, Video 10, bottom) WT meiosis II embryos treated with 150 μg/ml BFA (n = 14). Arrows mark the positions of the two centrosomes. Schematic representations of the movements of the posterior centrosome during pronuclear centration are drawn. Scale bar, 10 μm.

the ER. One possibility is that proteins regulating metaphase MT length could be processed and transported via the ER, whose normal morphology requires functional RAB-11 (this study). Our failure to demonstrate any mislocalization of MAPs in RAB-11 depleted embryos (see above) makes this possibility somewhat less likely.

It has been shown that ER-regulated calcium levels can alter MT dynamics (Facanha *et al.*, 2002). Thus, as the ER cycles from its reticulate organization during metaphase to dispersed structures during anaphase (Poteryaev *et al.*, 2005), it could provide cell-cycle–specific regulation of free calcium levels, which would affect MT growth or stability. In

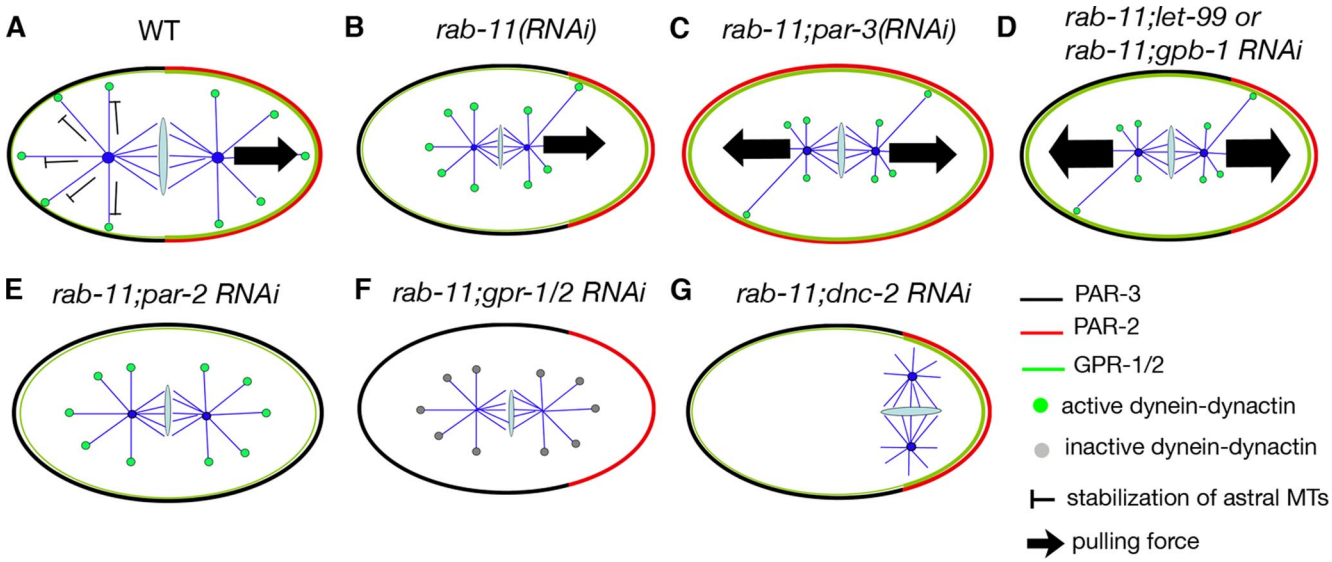

Figure 9. Model for the violent spindle movements in *rab-11(RNAi)* embryos. In the WT embryo (A), the posterior pulling force at metaphase is balanced by the tethering of astral MTs at the anterior cortex (Labbe *et al.*, 2004). In the *rab-11(RNAi)* embryo (B), the metaphase MTs are short and no longer stabilized at the anterior, subjecting the spindle only to the pulling force from the posterior. The longer MT represents the few that do manage to reach to the posterior cortex where more abundant GPR-1/2 localizes, so that dynein-dynactin (shown in green dots) can exert pulling forces on the spindle. In the *rab-11; par-3(RNAi)* embryo (C), GPR-1/2 level is evenly elevated around the cortex (Colombo *et al.*, 2003; Gotta *et al.*, 2003). The spindle is then under equal pulling forces from both poles, and it undergoes violent movements in the center of the embryo. In the *rab-11; let-99(RNAi)* or *rab-11; gpb-1(RNAi)* embryo (D), the GPR-1/2 activity may be further up-regulated due to the disruption of these antagonizing regulators of G_{α} (Tsou *et al.*, 2003), which results in even stronger pulling forces. Furthermore, because the embryo is still polarized, unlike in the *rab-11; par-3(RNAi)* embryo, the pulling forces may be unbalanced (not shown in the diagram) and thus lead to more violent and unpredictable spindle movements. The pulling force from the cortex is suppressed in the *rab-11; par-2(RNAi)* embryo (E) due to reduced GPR-1/2 activity (Colombo *et al.*, 2003; Gotta *et al.*, 2003). In the *rab-11; gpr-1/2(RNAi)* embryo (F), both GPR-1/2 and dynein-dynactin activities are reduced (Grill *et al.*, 2003), accounting for the absence of pulling force from the posterior cortex. Inactivating the motor dynein-dynactin in *rab-11; dnc-2(RNAi)* embryo (G) also suppresses the pulling force from the cortex even though the GPR-1/2 activity may be normal.

this scheme, RAB-11 could act directly in calcium regulation (such as interacting with a Ca^{2+} channel; van de Graaf *et al.*, 2006) or indirectly (by affecting ER morphology, thereby regulating calcium levels in microdomains) to stabilize metaphase astral MTs.

When the ER disperses at the metaphase-to-anaphase transition, MTs become subject to different forms of cell-cycle–dependent regulation, such as by ZYG-8. Interestingly, we found that the ER also forms large aggregates during metaphase in *zyg-8(b235)* embryos. However, unlike in *rab-11(RNAi)* embryos, these aggregates persisted through anaphase. If the ER is regulating MT length, this may explain why *zyg-8* mutant embryos exhibit defects in anaphase MT assembly (Gonczy *et al.*, 2001), as well as a slight reduction in the MT growth during metaphase (Srayko *et al.*, 2005). Possibly the doublecortin ZYG-8 may change MT dynamics in correspondence to the ER cycle. Although it is not known whether ZYG-8 is associated with the ER, it has been found that the chicken ortholog of ZYG-8 is associated with membrane structures (Capes-Davis *et al.*, 2005). In genes that affect MT length independently of the cell cycle, such as *zyg-9* (Matthews *et al.*, 1998), the ER morphology was normal when these genes were depleted (Figure 8, G and H).

Our observations indicate that the length of astral MTs during metaphase is at least partially determined by RAB-11. The stage-specific perturbation of ER structure seen upon RAB-11 depletion suggests that the ER may in some way determine the length of astral MTs at metaphase. However, the depletion of RAB-11 must perturb the ER in a specific way because depletion of other proteins, such as CAR-1, can produce superficially similar disruptions of ER morphology without causing the shortened astral MTs or spindle alignment defects observed with RAB-11 depletion (Squirrell *et al.*, 2006). Furthermore, depletion of the ER proteins OOC-3 and -5 as well as BFA treatment can cause perturbations of ER structure and spindle alignment defects without any concomitant shortening of MTs during metaphase. We should also mention that a normal ER organization alone is not sufficient to permit proper spindle alignment. For genes required for spindle alignment that regulate the interactions between the astral MTs and cortex, such as *let-99* (Tsou *et al.*, 2002; Tsou *et al.*, 2003) and the trimeric G proteins (Labbe *et al.*, 2003), the ER morphology was normal when these genes were depleted. However, given that nocodazole-mediated shortening of MTs during metaphase is sufficient to phenocopy the spindle alignment phenotype of RAB-11 depletion, we speculate that RAB-11 acts permissively (possibly via the ER) to specify an appropriate length for astral MTs at metaphase to allow the cortical interactions that mediate the alignment of the mitotic spindle.

ACKNOWLEDGMENTS

We thank Koen Verbrugghe and Sebastian Bednarek for discussion and comments on the manuscript. We are grateful to Drs. Yuji Kohara and Dmitry Poteryaev and to Anne Spang, Chris Malone, Susan Strome, Geraldine Seydoux, Ken Kemphues, Tony Hyman, Pierre Gönczy, Iva Greenwald, Yun Chi, David Ron, and Judith Kimble, as well as the *Caenorhabditis* Genetics Center and Developmental Studies Hybridoma Bank for reagents and use of equipment. We also thank Bharti Solanki for constructing the *gfp::nmy-2* strain used for the studies described in the supplement. This work was supported by the National Institutes of Health Grant GM052454-09 J.G.W.

REFERENCES

Basham, S. E., and Rose, L. S. (1999). Mutations in *ooc-5* and *ooc-3* disrupt oocyte formation and the reestablishment of asymmetric PAR protein localization in two-cell *Caenorhabditis elegans* embryos. Dev. Biol. *215*, 253–263.

Basham, S. E., and Rose, L. S. (2001). The *Caenorhabditis elegans* polarity gene *ooc-5* encodes a Torsin-related protein of the AAA ATPase superfamily. Development *128*, 4645–4656.

Brenner, S. (1974). The genetics of *Caenorhabditis elegans*. Genetics *77*, 71–94.

Boyd, L., Guo, S., Levitan, D., Stinchcomb, D. T., and Kemphues, K. J. (1996). PAR-2 is asymmetrically distributed and promotes association of P granules and PAR-1 with the cortex in *C. elegans* embryos. Development *122*, 3075–3084.

Capes-Davis, A., Tolhurst, O., Dunn, J. M., and Jeffrey, P. L. (2005). Expression of doublecortin (DCX) and doublecortin-like kinase (DCLK) within the developing chick brain. Dev. Dyn. *232*, 457–467.

Colombo, K., Grill, S.W., Kimple, R. J., Willard, F. S., Siderovski, D. P., and Gonczy, P. (2003). Translation of polarity cues into asymmetric spindle positioning in *Caenorhabditis elegans* embryos. Science *300*, 1957–1961. Epub 2003 May 1915.

Cowan, C. R., and Hyman, A. A. (2004a). Asymmetric cell division in *C. elegans*: cortical polarity and spindle positioning. Annu. Rev. Cell Dev. Biol. *20*, 427–453.

Cowan, C. R., and Hyman, A. A. (2004b). Centrosomes direct cell polarity independently of microtubule assembly in *C. elegans* embryos. Nature *431*, 92–96.

Dollar, G., Struckhoff, E., Michaud, J., and Cohen, R. S. (2002). Rab11 polarization of the *Drosophila* oocyte: a novel link between membrane trafficking, microtubule organization, and oskar mRNA localization and translation. Development *129*, 517–526.

Encalada, S. E., Willis, J., Lyczak, R., and Bowerman, B. (2005). A spindle checkpoint functions during mitosis in the early *Caenorhabditis elegans* embryo. Mol. Biol. Cell *16*, 1056–1070. Epub 2004 Dec 1022.

Etemad-Moghadam, B., Guo, S., and Kemphues, K. J. (1995). Asymmetrically distributed PAR-3 protein contributes to cell polarity and spindle alignment in early *C. elegans* embryos. Cell *83*, 743–752.

Facanha, A. L., Appelgren, H., Tabish, M., Okorokov, L., and Ekwall, K. (2002). The endoplasmic reticulum cation P-type ATPase Cta4p is required for control of cell shape and microtubule dynamics. J. Cell Biol. *157*, 1029–1039. Epub 2002 Jun 1010.

Fire, A., Xu, S., Montgomery, M. K., Kostas, S. A., Driver, S. E., and Mello, C. C. (1998). Potent and specific genetic interference by double-stranded RNA in *Caenorhabditis elegans*. Nature *391*, 806–811.

Goldstein, B. (2000). When cells tell their neighbors which direction to divide. Dev. Dyn. *218*, 23–29.

Gonczy, P., Bellanger, J. M., Kirkham, M., Pozniakowski, A., Baumer, K., Phillips, J. B., and Hyman, A. A. (2001). *zyg-8*, a gene required for spindle positioning in *C. elegans*, encodes a doublecortin-related kinase that promotes microtubule assembly. Dev. Cell *1*, 363–375.

Gonczy, P., Pichler, S., Kirkham, M., and Hyman, A. A. (1999a). Cytoplasmic dynein is required for distinct aspects of MTOC positioning, including centrosome separation, in the one cell stage *Caenorhabditis elegans* embryo. J. Cell Biol. *147*, 135–150.

Gonczy, P., Schnabel, H., Kaletta, T., Amores, A. D., Hyman, T., and Schnabel, R. (1999b). Dissection of cell division processes in the one cell stage *Caenorhabditis elegans* embryo by mutational analysis. J. Cell Biol. *144*, 927–946.

Gotta, M., and Ahringer, J. (2001). Distinct roles for Galpha and Gbetagamma in regulating spindle position and orientation in *Caenorhabditis elegans* embryos. Nat. Cell Biol. *3*, 297–300.

Gotta, M., Dong, Y., Peterson, Y. K., Lanier, S. M., and Ahringer, J. (2003). Asymmetrically distributed *C. elegans* homologs of AGS3/PINS control spindle position in the early embryo. Curr. Biol. *13*, 1029–1037.

Grant, B., Zhang, Y., Paupard, M. C., Lin, S. X., Hall, D. H., and Hirsh, D. (2001). Evidence that RME-1, a conserved *C. elegans* EH-domain protein, functions in endocytic recycling. Nat. Cell Biol. *3*, 573–579.

Grill, S. W., Howard, J., Schaffer, E., Stelzer, E. H., and Hyman, A. A. (2003). The distribution of active force generators controls mitotic spindle position. Science *301*, 518–521.

Hales, C. M., Griner, R., Hobdy-Henderson, K. C., Dorn, M. C., Hardy, D., Kumar, R., Navarre, J., Chan, E. K., Lapierre, L. A., and Goldenring, J. R. (2001). Identification and characterization of a family of Rab11-interacting proteins. J. Biol. Chem. *276*, 39067–39075.

Hobdy-Henderson, K. C., Hales, C. M., Lapierre, L. A., Cheney, R. E., and Goldenring, J. R. (2003). Dynamics of the apical plasma membrane recycling system during cell division. Traffic *4*, 681–693.

Horgan, C. P., Walsh, M., Zurawski, T. H., and McCaffrey, M. W. (2004). Rab11-FIP3 localises to a Rab11-positive pericentrosomal compartment during interphase and to the cleavage furrow during cytokinesis. Biochem. Biophys. Res. Commun. *319*, 83–94.

Hung, T. J., and Kemphues, K. J. (1999). PAR-6 is a conserved PDZ domain-containing protein that colocalizes with PAR-3 in *Caenorhabditis elegans* embryos. Development *126*, 127–135.

Jones, M. C., Caswell, P. T., and Norman, J. C. (2006). Endocytic recycling pathways: emerging regulators of cell migration. Curr. Opin. Cell Biol. *18*, 549–557.

Kamath, R. S. *et al*. (2003). Systematic functional analysis of the *Caenorhabditis elegans* genome using RNAi. Nature *421*, 231–237.

Kemphues, K. J., Kusch, M., and Wolf, N. (1988). Maternal-effect lethal mutations on linkage group II of *Caenorhabditis elegans*. Genetics *120*, 977–986.

Labbe, J. C., Maddox, P. S., Salmon, E. D., and Goldstein, B. (2003). PAR proteins regulate microtubule dynamics at the cell cortex in *C. elegans*. Curr. Biol. *13*, 707–714.

Labbe, J. C., McCarthy, E. K., and Goldstein, B. (2004). The forces that position a mitotic spindle asymmetrically are tethered until after the time of spindle assembly. J. Cell Biol. *167*, 245–256. Epub 2004 Oct 2018.

Lindsay, A. J., Hendrick, A. G., Cantalupo, G., Senic-Matuglia, F., Goud, B., Bucci, C., and McCaffrey, M. W. (2002). Rab coupling protein (RCP), a novel Rab4 and Rab11 effector protein. J. Biol. Chem. *277*, 12190–12199.

Matthews, L. R., Carter, P., Thierry-Mieg, D., and Kemphues, K. (1998). ZYG-9, a *Caenorhabditis elegans* protein required for microtubule organization and function, is a component of meiotic and mitotic spindle poles. J. Cell Biol. *141*, 1159–1168.

Mello, C. C., Schubert, C., Draper, B., Zhang, W., Lobel, R., and Priess, J. R. (1996). The PIE-1 protein and germline specification in *C. elegans* embryos. Nature *382*, 710–712.

Morton, D. G., Shakes, D. C., Nugent, S., Dichoso, D., Wang, W., Golden, A., and Kemphues, K. J. (2002). The *Caenorhabditis elegans* par-5 gene encodes a 14-3-3 protein required for cellular asymmetry in the early embryo. Dev. Biol. *241*, 47–58.

Pelissier, A., Chauvin, J. P., and Lecuit, T. (2003). Trafficking through Rab11 endosomes is required for cellularization during *Drosophila* embryogenesis. Curr. Biol. *13*, 1848–1857.

Pichler, S., Gonczy, P., Schnabel, H., Pozniakowski, A., Ashford, A., Schnabel, R., and Hyman, A. A. (2000). OOC-3, a novel putative transmembrane protein required for establishment of cortical domains and spindle orientation in the P(1) blastomere of *C. elegans* embryos. Development *127*, 2063–2073.

Poteryaev, D., Fares, H., Bowerman, B., and Spang, A. (2007). *Caenorhabditis elegans* SAND-1 is essential for RAB-7 function in endosomal traffic. EMBO J. *26*, 301–312.

Poteryaev, D., Squirrell, J. M., Campbell, J. M., White, J. G., and Spang, A. (2005). Involvement of the actin cytoskeleton and homotypic membrane fusion in ER dynamics in *Caenorhabditis elegans*. Mol. Biol. Cell. *16*, 2139–2153. Epub 2005 Feb 2116.

Praitis, V., Casey, E., Collar, D., and Austin, J. (2001). Creation of low-copy integrated transgenic lines in *Caenorhabditis elegans*. Genetics *157*, 1217–1226.

Prekeris, R. (2003). Rabs, Rips, FIPs, and endocytic membrane traffic. Sci. World J. *3*, 870–880.

Riggs, B., Rothwell, W., Mische, S., Hickson, G. R., Matheson, J., Hays, T. S., Gould, G. W., and Sullivan, W. (2003). Actin cytoskeleton remodeling during early *Drosophila* furrow formation requires recycling endosomal components Nuclear-fallout and Rab11. J. Cell Biol. *163*, 143–154. Epub 2003 Oct 2006.

Shaw, S. L., and Quatrano, R. S. (1996). The role of targeted secretion in the establishment of cell polarity and the orientation of the division plane in *Fucus* zygotes. Development *122*, 2623–2630.

Shelton, C. A., and Bowerman, B. (1996). Time-dependent responses to glp-1-mediated inductions in early *C. elegans* embryos. Development *122*, 2043–2050.

Skop, A. R., Bergmann, D., Mohler, W. A., and White, J. G. (2001). Completion of cytokinesis in *C. elegans* requires a brefeldin A-sensitive membrane accumulation at the cleavage furrow apex. Curr. Biol. *11*, 735–746.

Skop, A. R., and White, J. G. (1998). The dynactin complex is required for cleavage plane specification in early *Caenorhabditis elegans* embryos. Curr. Biol. *8*, 1110–1116.

Squirrell, J. M., Eggers, Z. T., Luedke, N., Saari, B., Grimson, A., Lyons, G. E., Anderson, P., and White, J. G. (2006). CAR-1, a protein that localizes with the mRNA decapping component DCAP-1, is required for cytokinesis and ER organization in *Caenorhabditis elegans* embryos. Mol. Biol. Cell *17*, 336–344. Epub 2005 Nov 2002.

Srayko, M., Kaya, A., Stamford, J., and Hyman, A. A. (2005). Identification and characterization of factors required for microtubule growth and nucleation in the early *C. elegans* embryo. Dev. Cell *9*, 223–236.

Sulston, J. E., Schierenberg, E., White, J. G., and Thomson, J. N. (1983). The embryonic cell lineage of the nematode *Caenorhabditis elegans*. Dev. Biol. *100*, 64–119.

Tagawa, A., Rappleye, C. A., and Aroian, R. V. (2001). Pod-2, along with pod-1, defines a new class of genes required for polarity in the early *Caenorhabditis elegans* embryo. Dev. Biol. *233*, 412–424.

Timmons, L., and Fire, A. (1998). Specific interference by ingested dsRNA. Nature *395*, 854.

Tsou, M. F., Hayashi, A., DeBella, L. R., McGrath, G., and Rose, L. S. (2002). LET-99 determines spindle position and is asymmetrically enriched in response to PAR polarity cues in *C. elegans* embryos. Development *129*, 4469–4481.

Tsou, M. F., Hayashi, A., and Rose, L. S. (2003). LET-99 opposes Galpha/GPR signaling to generate asymmetry for spindle positioning in response to PAR and MES-1/SRC-1 signaling. Development *130*, 5717–5730. Epub 2003 Oct 5718.

Ullrich, O., Reinsch, S., Urbe, S., Zerial, M., and Parton, R. G. (1996). Rab11 regulates recycling through the pericentriolar recycling endosome. J. Cell Biol. *135*, 913–924.

van de Graaf, S. F., Chang, Q., Mensenkamp, A. R., Hoenderop, J. G., and Bindels, R. J. (2006). Direct interaction with Rab11a targets the epithelial Ca^{2+} channels TRPV5 and TRPV6 to the plasma membrane. Mol. Cell. Biol. *26*, 303–312.

Voeltz, G. K., Rolls, M. M., and Rapoport, T. A. (2002). Structural organization of the endoplasmic reticulum. EMBO Rep. *3*, 944–950.

Wallace, D. M., Lindsay, A. J., Hendrick, A. G., and McCaffrey, M. W. (2002). Rab11-FIP4 interacts with Rab11 in a GTP-dependent manner and its overexpression condenses the Rab11 positive compartment in HeLa cells. Biochem. Biophys. Res. Commun. *299*, 770–779.

Walston, T. D., and Hardin, J. (2006). Wnt-dependent spindle polarization in the early *C. elegans* embryo. Semin. Cell Dev. Biol. *17*, 204–213.

Watts, J. L., Morton, D. G., Bestman, J., and Kemphues, K. J. (2000). The *C. elegans par-4* gene encodes a putative serine-threonine kinase required for establishing embryonic asymmetry. Development *127*, 1467–1475.

Wilson, G. M., Fielding, A. B., Simon, G. C., Yu, X., Andrews, P. D., Hames, R. S., Frey, A. M., Peden, A. A., Gould, G. W., and Prekeris, R. (2005). The FIP3-Rab11 protein complex regulates recycling endosome targeting to the cleavage furrow during late cytokinesis. Mol. Biol. Cell *16*, 849–860.

Wokosin, D. L., Squirrell, J. M., Eliceiri, K. W., and White, J. G. (2003). Optical workstation with concurrent, independent multiphoton imaging and experimental laser microbeam capabilities. Rev. Sci. Instrum. *74*, 1–9.

Wright, A. J., and Hunter, C. P. (2003). Mutations in a beta-tubulin disrupt spindle orientation and microtubule dynamics in the early *Caenorhabditis elegans* embryo. Mol. Biol. Cell *14*, 4512–4525. Epub 2003 Aug 4522.

Zerial, M., and McBride, H. (2001). Rab proteins as membrane organizers. Nat. Rev. Mol. Cell Biol. *2*, 107–117.